Proceedings of the 1st international Symposium on AI and Fluid Mechanics
Paper No S13 P1

Real-time feedback control of flow field behind a cylinder using sparse processing PIV and plasma actuators

R. Naramura[1], C. Abe[2], Y. Sasaki[3] and T. Nonomura[3]

[1]Department of Mechanical System Engineering, Nagoya University, Nagoya, Japan

[2] Department of Aerospace Engineering, Tohoku University, Sendai, Japan

[3]Department of Aerospace Engineering, Nagoya University, Nagoya, Japan

Keywords: Wind Tunnel Testing, Sparse Sensing, Particle Image Velocimetry, Feedback Control, Plasma Actuator

Abstract. As active fluid control methods for improving the flight performance of aircraft and other vehicles are gaining importance, fluid control using a plasma actuator (PA) has been attracting attention. Therefore, it is important to construct a feedback control system that determines the PA control inputs from the real-time observed flow field information. In this study, a real-time feedback control system to suppress the Karman vortex in the wake of a cylinder model was constructed using two PAs, and its control effect was investigated in wind tunnel experiments. For real-time observation of the flow field, sparse processing particle image velocimetry (SPPPV) method based on sparse sensing and proper orthogonal decomposition (POD) is used. The measured data was applied to a Kalman filter (KF) to estimate the flow field in real time and determine the optimal PA input. As a control law of PA, sum-of-absolute-value (SOAV) control was applied. The real-time control effect was evaluated in terms of frequency of POD mode coefficients and flow asymmetry. Two types of training data were used: updating data for each run and adding data. As a result, the effectiveness of real-time feedback control on suppression of the Karman vortex was confirmed.

1. Introduction

In recent years, the development of active fluid control methods for improving the flight performance of aircraft has become an important issue. Plasma actuator (PA) [1, 2, 3] is an active fluid control device that has attracted attention because of its simple structure and installation method, and its application in combination with feedback control is desired. To realize feedback control, it is necessary to observe the flow field in real-time, and data acquisition using methods such as particle image velocimetry (PIV) is considered [4]. However, the fluctuation of aerodynamic phenomena is generally fast [5], and real-time measurement of the flow field is very difficult. Kanda et al [6,7] proposed sparse processing PIV (SPPIV) , which is based on sparse sensing and proper orthogonal decomposition (POD), to realize real-time measurement. Abe et al. [8] constructed a feedback control system for a flow field around a circular cylinder by using a controller that drives two PAs with SPPIV as an observer, and achieved feedback control to suppress the Karman vortex in the wake in wind tunnel tests. However, the feedback control system with SPPIV and PA still has room for improvement, as it is not able to select control inputs based on parameter studies using information from the flow field in a controlled state. In this study, we investigate the change in control effectiveness by adding data from feedback control to the training data used for control system identification for the control systems constructed in previous studies.

2. Measurement Principles and Control Laws

2.1 Sparce processing PIV (SPPIV)

Figure 1 shows a schematic of the flow velocity field measurement using SPPIV proposed by Kanda et al [6, 7]. The velocity field is estimated from the obtained sparse velocity field using a Kalman filter (KF) based on a discrete-time linear model.

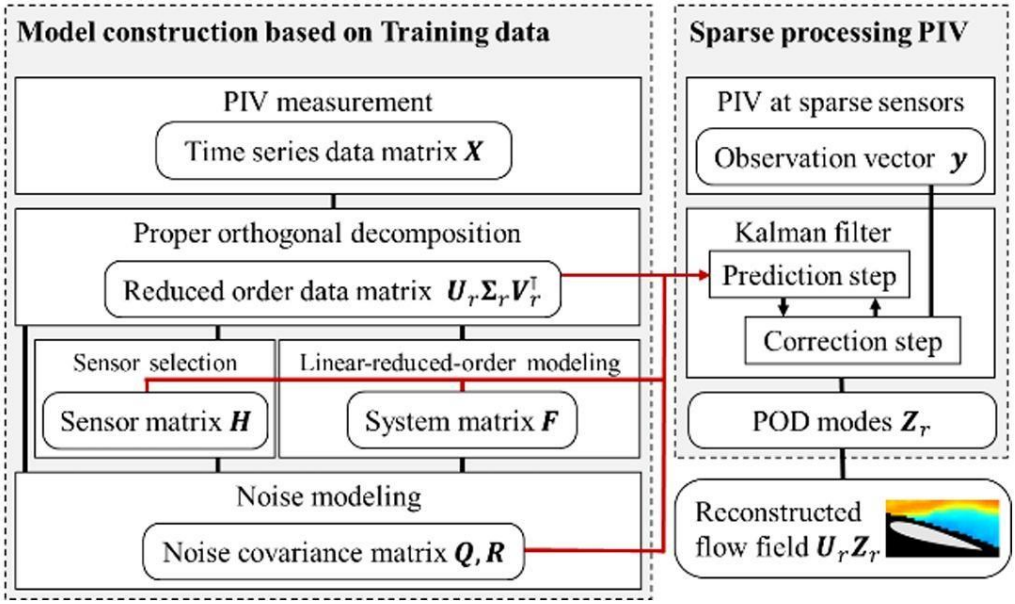

Figure 1. Flowchart of SPPIV [6]

In this study, the data matrix X storing the flow velocity field is transformed by POD into the following equation

$$X = U\Sigma V^{\mathrm{T}} \approx \underset{r}{U}\,\underset{r}{\Sigma}\,\underset{r}{V^T} \tag{1}$$

where $U \in \mathbb{R}^{M\times N}$, $\Sigma \in \mathbb{R}^{N\times N}$, and $V \in \mathbb{R}^{N\times N}$ are the spatial, amplitude, and temporal modes, respectively, and the upper r-mode approximations are denoted as $U_r \in \mathbb{R}^{M\times r}$, $\Sigma_r \in \mathbb{R}^{r\times r}$, and $V_r \in \mathbb{R}^{N\times r}$, respectively. In SPPIV, the time evolution $\boldsymbol{z} \in \mathbb{R}^r$ of the POD mode corresponding to each column of $\Sigma_r V_r^{\mathrm{T}}$ is calculated sequentially. The velocity field can be reconstructed by projecting the time-series data onto the spatial mode U_r, which is calculated beforehand based on ordinary PIV.

2.2 Low-dimensional modeling with linear models

Assume that the state $\boldsymbol{z}(k) \in \mathbb{R}^r$ follows. Let $\boldsymbol{z} \in \mathbb{R}^r$ denote the estimated state vector, $\boldsymbol{y}_{obs}(k) \in \mathbb{R}^{sp}$ the observed one, and $\boldsymbol{v}_{noise}(k) \in \mathbb{R}^r$ and $\boldsymbol{w}_{noise}(k) \in \mathbb{R}^{sp}$ the system noise and observed noise, respectively. where $s = 2$ is the dimensionality of the velocity field and p is the number of observation points.

$$\boldsymbol{z}(k+1) = F\boldsymbol{z}(k) + B\boldsymbol{u}(k-L) + \boldsymbol{v}_{noise}(k) \tag{2}$$

$$\boldsymbol{y}_{obs}(k) = C\boldsymbol{z}(k) + \boldsymbol{w}_{noise}(k) \tag{3}$$

The input $\boldsymbol{u}(k) \in \mathbb{R}^m$ is an $m(=2)$-dimensional vector of 1 and 0 corresponding to the ON and OFF of the two PAs, with values before time L to account for the time difference between the discharge and the flow field. The system matrix $F \in \mathbb{R}^{r\times r}$ and the input matrix $B \in \mathbb{R}^{r\times m}$ were calculated by dynamic mode decomposition with control (DMDc) [9]. $C \in \mathbb{R}^{sp\times r}$ in equation (3) is the observation matrix reflecting the observation point location information, and the observation point location optimization method for vector fields proposed by Saito et al [10, 11] was used. This method uses a greedy method to select observation point locations where multiple components are acquired at a single point. The determinant of the Fisher information matrix is used as the objective function, aiming to minimize the expected error variance in the

mode strength estimation. $\boldsymbol{v}_{noise}(k)$ and $\boldsymbol{w}_{noise}(k)$ are the residuals of substituting real data $\boldsymbol{z}$ and $\boldsymbol{y}_{obs}$ into the linear system. A linear non-stationary Kalman filter [12] was used for state estimation.

2.3 Feedback control law

In this study, the suppression of the Karman vortex in the wake of a cylindrical model is considered by reducing the antisymmetric spatial mode coefficients, which is the control target. Given an input $\boldsymbol{u}(k)$ at time k, the state $\boldsymbol{z}(k+L)$ after time L is estimated in a linear system as

$$\boldsymbol{z}(k+L) = F^{L}\boldsymbol{z}(k) + \sum_{i=1}^{L} F^{L-i}B\boldsymbol{u}(k+L-i) \tag{4}$$

Based on the linear model prediction by equation (4), sum-of-absolute-values optimization (SOAV) [13] is applied to the algorithm of the control law. In this method, a sparse control method based on the L_1 norm optimization problem is applied to find the discrete-valued control input that is considered optimal. The control input $\boldsymbol{v} = [\boldsymbol{u}(k)^{\mathrm{T}}\ \boldsymbol{u}(k+1)^{\mathrm{T}} \cdots \boldsymbol{u}(k+\nu-1)^{\mathrm{T}}]^{\mathrm{T}} \in \mathbb{R}^{m\nu}$ for the state $\boldsymbol{\xi} = \boldsymbol{z}(k+L)$ predicted by equation (4) and for the subsequent ν steps to approach the origin is expressed as follows. where $\mathbf{0}$ and $\mathbf{1}$ are vectors, whose total components are 0 and 1, $\boldsymbol{\zeta} = F^{\nu}\boldsymbol{\xi}$, $\Phi = [F^{\nu-1}B\ F^{\nu-2}B \cdots B]$.

$$\min_{\boldsymbol{v}}(\alpha \parallel \Phi\boldsymbol{v} + \boldsymbol{\zeta} \parallel_2^2 + |\boldsymbol{v} - \mathbf{0}| + |\boldsymbol{v} - \mathbf{1}|) \text{ subject to } 0 \le v_i \le 1 \tag{5}$$

In this study, the optimal input is obtained by iteratively computing the alternating direction method of multipliers (ADMM) [14]. To apply ADMM to the optimization problem (5) with constraints on the range of variables, problem (5) was rewritten as follows using the variables $\boldsymbol{y} = [\boldsymbol{y}_0^{\mathrm{T}}\ \boldsymbol{y}_1^{\mathrm{T}}\ \boldsymbol{y}_2^{\mathrm{T}}]$ $(\boldsymbol{y}_i \in \mathbb{R}^{m\nu})$ and $\boldsymbol{\Psi} = [I\ I\ I]^{\mathrm{T}} \in \mathbb{R}^{3m\nu \times m\nu}$ with $\boldsymbol{v}$ extended

$$\min_{\boldsymbol{v}}(\alpha \parallel \Phi\boldsymbol{v} + \boldsymbol{\zeta} \parallel_2^2 + |\boldsymbol{y}_0 - \mathbf{0}| + |\boldsymbol{y}_1 - \mathbf{1}| + \iota(\boldsymbol{y}_2)) \text{ subject to } \boldsymbol{y} = \boldsymbol{\Psi}\boldsymbol{v} \tag{6}$$

where $\iota(\boldsymbol{x})$ is an indicator function that returns 0 if $0 \le x_i \le 1$ for all i and ∞ otherwise. $\boldsymbol{w} = [\boldsymbol{w}_0^{\mathrm{T}}\ \boldsymbol{w}_1^{\mathrm{T}}\ \boldsymbol{w}_2^{\mathrm{T}}]$ $(\boldsymbol{w}_i \in \mathbb{R}^{m\nu})$, $S_{\gamma}(\boldsymbol{x})$ is a soft threshold function, $sat(\boldsymbol{x})_i$ is a saturation function that returns x_i when $0 \le x_i \le 1$. $sat(\boldsymbol{x})_i$ returns 0 and 1 when $x_i < 0$ and $1 < x_i$, respectively.

3. Experimental methods

A schematic diagram of the experimental setup used in this study is shown in figure 2. The experiment was conducted in the Nagoya University Basic Aerodynamic Research Tunnel (NU-BART), using a plastic cylinder model (diameter 30 mm, width 300 mm) with two PAs installed. The high-speed camera used in this study was an IDP-Express R2000 from Photron. The main flow velocity was 5 m/s, and the shooting speed during PIV measurement was 4,000 fps. The PAs were installed as shown in figure 2 and driven by a PSI-PA1050N high-voltage output amplifier from P.S.I. The waveform of the PAs was set to a sine wave of 10,000 Hz and 8 kVpp and discharged only during the ON state. The two PAs were operated independently of each other. The number of estimated modes was set to 2 ($r = 2$). For real-time control, the number of observation points p was set to 5, and the PA was controlled by the digital output of a National Instrument PCIe-6323 I/O device embedded in a computer. In equation (6), α was set to 0.5 and ν to 40. In this experiment, a total of 10,000 pairs of particle images were acquired under conditions in which the PA was randomly switched on and off at 100 Hz, and PIV analysis was used to generate training data.

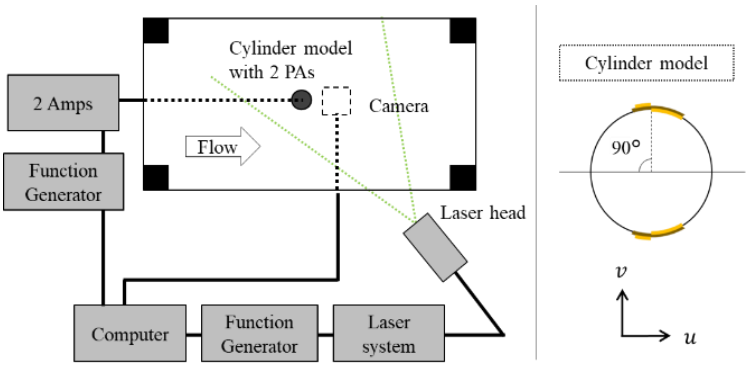

Figure 2. Experimental setup

In this experiment, we investigated the case of changing the training data used for determining the position of observation points and system identification in SPPIV. For the first feedback control, training data was generated by PIV analysis of a total of 10,000 pairs of particle images acquired under conditions in which the PA was randomly switched on and off at 100 Hz. In subsequent experiments, two conditions were used. The first was the case where the velocity field data from the feedback control was updated and used as new training data. The data from the feedback control was defined as "run 1", and the new data was used as the training data to obtain the data of "run 2". This process was continued until run 6 data was obtained. In the second case, the velocity field data from the feedback control was added to the previous training data and used as the new training data. The experiment was conducted by adding this data to the randomly discharged velocity field data and using it as new training data for feedback control to obtain the run 2 data, and this operation was continued until the run 6 data was obtained. When feedback control was performed using the same training data, 10 times of data were acquired, and the training data with the greatest control effect was used as the next training data.

4. Results and discussion

4.1 Visualization results of feedback control results

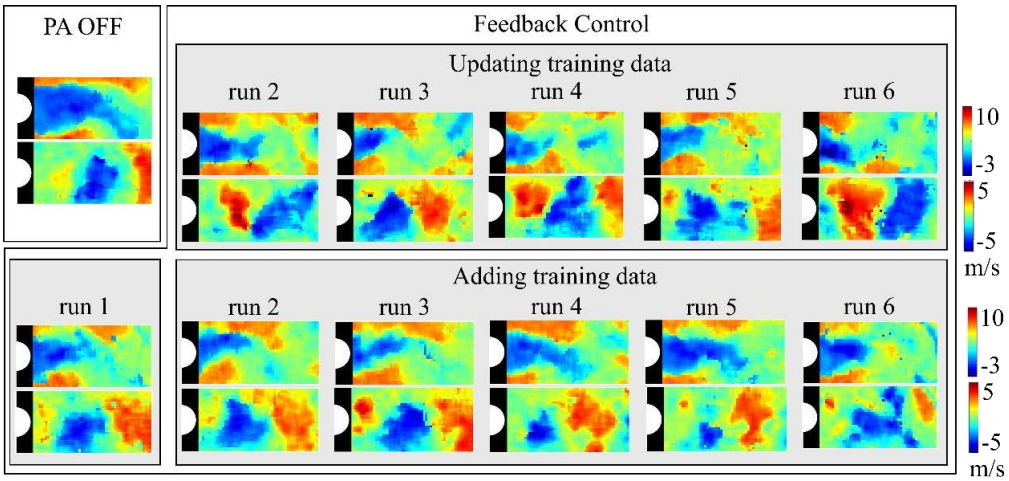

Figure 3. Flow velocity field at each control

Figure 3 shows the velocity field with PA always turned off and the velocity field during feedback control under each condition. The upper panel shows the flow velocity in the main flow direction and the lower

panel shows the flow velocity in the vertical flow direction. The figure shows the instantaneous velocity field at dimensionless time $tU_\infty/d = 100$, which is non-dimensionalized by the main flow velocity U_∞ and the cylinder diameter d. Switching the PA on and off by feedback control qualitatively disturbed the large-scale structure of the velocity field and reduced the recirculation area. Since the recirculation area is reduced in all cases, differences in control effects due to changes in the training data cannot be discerned from the visualization.

4.2 Quantitative evaluation of control effectiveness

In this study, the control effect was evaluated by the symmetry of the velocity field normalized by the mainstream velocity. For the $H \times W$ wake region where the Karman vortex fully appears (in this study, 30×30, which is half of the angle of view, was used), $Asym.$ as a measure of asymmetry was defined as follows

$$Asym. = \sum_{i=1}^{W} \sum_{j=1}^{H/2} \left(\left(\frac{u_{i,j} - u_{i,H-j}}{U_\infty} \right)^2 + \left(\frac{v_{i,j} + v_{i,H-j}}{U_\infty} \right)^2 \right) \quad (7)$$

Figure 4 shows the mean and standard deviation of $Asym.$ without control, with random discharge, and with feedback control under each condition. (a) shows the results when the training data is updated, and (b) shows the results when the training data is added. Each data set is calculated as the average of the top five data sets in which the control effect was significant. Both graphs show that the $Asym.$ values are smaller in the case of feedback control than in the case of no control or random discharge. Furthermore, the $Asym.$ value was smaller and the variance was smaller when the training data was added, suggesting that the control effects were more stable.

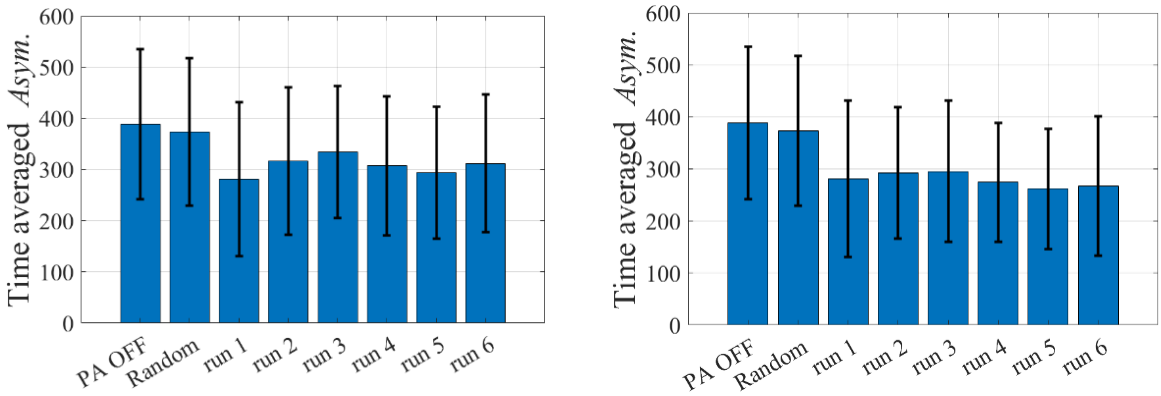

Figure 4. Time averaged $Asym.$ at each control

Figure 5 shows the cumulative energy of the POD mode coefficients for each data set. (a) shows the results when the training data is updated, and (b) shows the results when the training data is added. As in the $Asym.$ graph, each data set is calculated as the average of the top five data sets with the largest control effect. When updating the training data, the cumulative energy fluctuates greatly from one data set to another, but when adding additional training data, it tends to converge to a constant value. The addition of the training data reproduces a similar flow field for each feedback control, indicating that the addition of training data is an effective method for stable control.

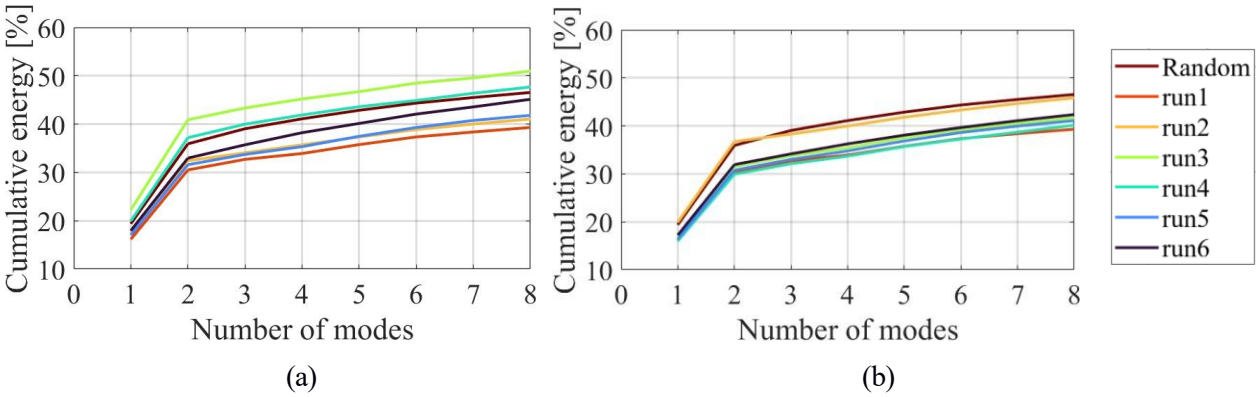

Figure 5. Cumulative energy at each control

Conclusion

In this study, we compared the flow field feedback control system using SPPIV as an observer with and without updating the training data used in the system. The control effect was quantitatively evaluated and confirmed for both conditions, but it was clarified that stable control with small dispersion was achieved when additional training data were used. In the future, we aim to achieve more efficient control by changing the current control law, which suppresses the L_2 norm of mode coefficients for single steps only, and by suppressing multi-step mode coefficients.

References

[1] H. Aono, S. Kawai, T. Nonomura, M. Sato, K. Fujii, K. Okada, 'Plasma-actuator burst-mode frequency effects on leading-edge flow-separation control at reynolds number 2.6× 10^5', AIAA Journal (2017) 3789–3806.

[2] T. C. Corke, M. L. Post, D. M. Orlov, 'Sdbd plasma enhanced aerodynamics: concepts, optimization and applications', Progress in Aerospace Sciences 43 (7-8) (2007) 193–217. doi:10.1016/j.paerosci.2007.06.001.

[3] A. Komuro, K. Takashima, K. Suzuki, S. Kanno, T. Nonomura, T. Kaneko, A. Ando, K. Asai,' Gas-heating phenomenon in a nanosecond pulse discharge in atmospheric-pressure air and its application for high-speed flow control', Plasma Sources Science and Technology 28 (6) (2019) 065006. doi:10.1088/1361-6595/ab1daf. URL

[4] T. Segawa, D. Suzuki, T. Fujino, T. Jukes, T. Matsunuma,'Feedback control of flow separation using plasma actuator and fbg sensor', International Journal of Aerospace Engineering 2016 (2016).

[5] J. T. Pinier, J. M Ausseur, M.N. Glauser, H. Higuchi, 'Proportional Closed-Loop Feedback Control of Flow Separation', AIAA Journal (2007) 181–190.

[6] N. Kanda, C. Abe, S. Goto, K. Yamada, K. Nakai, Y. Saito, K. Asai, T. Nonomura, 'Proof of-concept study of sparse processing particle image velocimetry for real time flow observation', Experiments of Fluids 63 (9) (2022).

[7] N. Kanda, K. Nakai, Y. Saito, T. Nonomura, K. Asai, 'Feasibility study on real-time observation of flow velocity field using sparse processing particle image velocimetry', Transactions of the Japan Society for Aeronautical and Space Sciences 64 (4) (2021) 242–245.

[8] C. Abe, Real-time Feedback Control of Flow Velocity Field Using Sparse Processing PIV and Plasma Actuators', master's thesis, Tohoku University, Japan, 2024

[9] J. L. Proctor, S. L. Brunton, J. N. Kutz, 'Dynamic mode decomposition with control', SIAM Journal on Applied Dynamical Systems 15 (1) (2016) 142–161.

[10] Y. Saito, K. Yamada, N. Kanda, K. Nakai, T. Nagata, T. Nonomura, K. Asai, 'Data-driven determinant-based greedy under/oversampling vector sensor placement', CMES-COMPUTER MODELING IN ENGINEERING & SCIENCES 129 (1) (2021) 1–30.

[11] Y. Saito, T. Nonomura, K. Nankai, K. Yamada, K. Asai, Y. Sasaki, D. Tsubakino, 'Data-driven vector-measurement-sensor selection based on greedy algorithm', IEEE Sensors Letters 4 (2020).

[12] 'Fundamentals of Kalman filter', Tokyo Denki University Press, 2010; Editors: S. Adachi, I. Maruta

[13] T. Ikeda, M. Nagahara, S. Ono, 'Discrete-valued control of linear time-invariant systems by sum of-absolute-values optimization', IEEE Transactions on Automatic Control 62 (6) (2017) 2750 2763. doi:10.1109/TAC.2016.2627683.

[14] S. Boyd, N. Parikh, E. Chu, Distributed optimization and statistical learning via the alternating direction method of multipliers', Now Publishers Inc, 2011